Nanoscale

Paper

Received 00th January 20xx,
Accepted 00th January 20xx

DOI: 10.1039/x0xx00000x

www.rsc.org/

A morphological, enzymatic and metabolic approach to elucidate apoptotic-like cell death in fungi exposed to *h*- and α- molybdenum trioxide nanoparticles

Clemencia Chaves-Lopez [a‡], Hang N. Nguyen[b‡], Rodrigo C. Oliveira[c‡], Enrico T. Nadres[b], Antonello Paparella[a], Debora F. Rodrigues[b*]

The present study compares for the first time the effects of *h*-MoO_3 and *α*-MoO_3 against two fungal strains: *Aspergillus niger* and *Aspergillus flavus*. The *h*-MoO_3 nanoparticle was more toxic to both fungi than *α*-MoO_3. The toxic effects of *h*-MoO_3 were more pronounced toward *A. flavus*, which presented a growth inhibition of 67.4% at 200 mg L^{-1}. The presence of the nanoparticles affected drastically the hyphae morphology by triggering nuclear condensation and compromising the hyphae membrane. Further analysis of the volatile organic compounds (VOCs) produced by both fungi in the presence of the nanomaterials indicated important metabolic changes related to programmed cell death. These nanomaterials induced the production of specific antifungal VOCs, such as β –Elemene and t-Cadinol, by fungi. The production of essential enzymes involved in fungal metabolism, such as acid phosphatase, naphthol-As-BI-phosphohydrolase, ß-galactosidase, ß-glucosidase and N-acetyl-ß-glucosaminidase, reduced significantly in the presence of the nanomaterials. The changes in enzymatic production and VOCs corroborate the fact that these nanoparticles, especially *h*-MoO_3, exert changes in the fungal metabolism, triggering apoptotic-like cell death responses in these fungi.

Introduction

Molybdenum trioxide (MoO_3) is a metal oxide semiconductor with a wide band gap and large surface area.[1, 2] The crystal structure of MoO_3 has three basic morphological phases: orthorhombic (*α*-MoO_3), monoclinic (*β*-MoO_3) and hexagonal (*h*-MoO_3).[3] However, two of them have caught the interest of the scientific community: metastable phase (*h*-MoO_3) and stable phase (α-MoO_3). These two structures have a broad range of applications in photocatalysis, oxidative catalysis, supercapacitors, coatings and as additive for paints;[2, 4] due to their active contribution to various reactions, such as redox reactions, selective oxidations or hydrogenation.[5] In addition, MoO_3 was found to be an effective antimicrobial against different bacterial strains.[6-9] However, the toxicity of these nanomaterials toward fungi is largely unknown. Just recently, a study by Fakhri and Nejad 2016 showed that *h*-MoO_3 had the potential to be antifungal. In this study, the authors only looked at zone of growth inhibition with a concentration extremely high (10,000 mg L^{-1}).[10] In this study, the authors did not explore the mechanisms of growth inhibition or the physiological responses of the fungi in the presence of *h*-MoO_3 or other MoO_3 nanomaterials. In order to fill this gap of knowledge, in the present study we present the toxicity of *h* and *α*- MoO_3 against *Aspergillus niger* and *Aspergillus flavus,* in concentrations varying from 0 to 200 mg L^{-1}. To complement the previously observed growth inhibition caused by MoO_3, the fungal metabolic and physiological responses were also investigated through observations of hyphae morphology, cell

[a.] *Facoltà di Bioscenze e Tecnologie Agroalimentari ed ambientali, Università degli Studi di Teramo, Via R. Balzarini 1 64100 Teramo, Italy.*
[b.] *Department of Civil and Environmental Engineering, University of Houston, Houston, TX 77204 – 4003 (U.S.A.)*
**Corresponding Author's Email: dfrigirodrigues@uh.edu Phone: +1-713-743-1495*
[c.] *Departament of Microbiology, University of Sao Paulo, Sao Paulo, Brazil.*
[‡] *These authors contributed equally to this work*
† Electronic Supplementary Information (ESI) available: [details of any supplementary information available should be included here]. See DOI: 10.1039/x0xx00000x

apoptosis and reactive oxygen species released from the hyphae. Additionally, the production of extracellular enzymes and volatile organic compounds (VOCs) by the fungi were also investigated to gain a better understanding of the changes of the fungal metabolism in the presence and absence of the nanoparticles and determine the adverse effects of different MoO_3 in different model fungi of the genus *Aspergillus*. The selection of *Aspergillus* was because species of this genus occur worldwide and have been isolated from various environments, they are specially abundant in the air due to their high production of conidia.[11, 12] The two *Aspergillus* species used in this study are *A. niger* and *A. flavus*. These species are clustered in two different sections: *Nigri* and *Flavi,* which are the two most important members of the *Aspergillus* genus. *Niger* and *flavus* are separated into sections due to their high genomic and functional diversity. The diversity of these two sections will reflect directly in different physiological traits, such as carbon utilization, secondary metabolism, and stress response.[7] Thus, the two selected species of *Aspergillus* are expected to have very distinctive responses to the two nanoparticles.[14] Furthermore, these two fungi are known to cause several diseases in crops, insects, animals and humans.[12, 15] They can spread fast and uncontrollably due to release of trillions of conidia per day as well as their ability to produce mycotoxins.[12, 16-18] These fungi are also highly resistant to most of the common antifungal and can survive a wide range of temperatures and pH.[19] These resistant characteristics are very attractive for model organisms to investigate antifungal properties of nanoparticles. In the present study, we hypothesize that *h*-MoO_3 will have higher toxicity than the α-MoO_3 against fungi. The rationale for this hypothesis is that the metastable phase of *h*-MoO_3 contains ammonium ions and water molecules that makes *h*-MoO_3 present higher electrical and ionic conductivity than α-MoO_3, which could interfere directly with the normal electrochemical potential of the cells. Furthermore, the hexagonal rod shape (needle-like shape) of the *h*-MoO_3 will allow a more effective interaction with the cell surface than α-MoO_3, which has plate-like structure. A needle-like shape will most likely lead to higher cellular damage than platelet shapes.

Results and discussion

Nanomaterial characterizations

The *h*-MoO_3 was synthesized by precipitation from acidified ammonium molybdate solution.[20, 21] In order to confirm the successful synthesis of *h*-MoO_3 and *α*-MoO_3 nanomaterials, X-ray diffraction (XRD), X-ray Photoelectron Spectroscopy (XPS), scanning electron microscopy (SEM), Raman spectroscopy and Fourier transform infrared attenuated total reflection (FTIR-ATR) analyses were performed. The XRD results showed that our nanomaterials exhibited the relevant diffractive peaks of MoO_3 (Fig. 1).[1, 20] The *α*-MoO_3 XRD spectra indicated a single phase of *α* without the mix of the *h* phase. Both *h* and *α*-MoO_3 showed distinctive peaks for their structures. For instance, the *h*-MoO_3 exhibited strong peaks at 9.7 (100), 19.6 (200), 25.9 (210) and 29.5 (300) of 2θ (Fig. 1), which are crystal planes of the *h* phase. In the case of *α*-MoO_3, the peaks showed the crystal planes of *α*-MoO_3 at 12.85 (020), 25.8 (040) and 39.1 (060) (Fig. 1).[3]

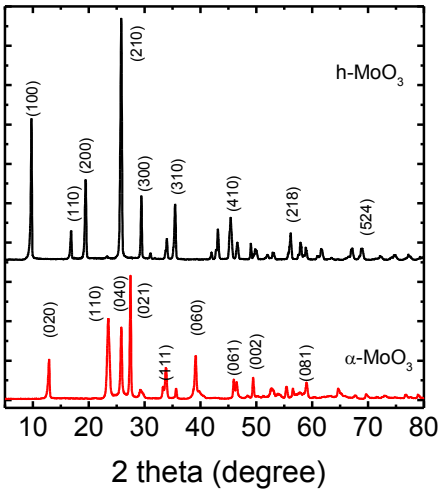

Fig 1. X-ray diffraction (XRD) spectra of h-MoO_3 and α-MoO_3, the spectra confirmed the successful synthesis of both MoO_3 structure with the characteristic peaks of each nanomaterial.[21]

The XPS confirmed the successful synthesis of *h*-MoO_3 and *α*-MoO_3 (Fig. 2). The characteristic peaks identified in XPS were assigned to the chemical states of MoO_3 based on previous investigations.[22, 23] The SEM analysis determined the structure and morphology of the crystals (Fig. 3). The *h*-MoO_3 obtained presented an orthorhombic structure characterized by hexagonal rod structures (Fig. 3), which is characteristic of *h*-MoO_3 as previously described in the literature.[3] The *h*-MoO_3 was successfully converted to *α*-MoO_3 at 500 °C for 8 h, since a layered orthorhombic structure was obtained (Fig. 3).[24, 25] The mode of the size frequency distribution for the rod diameter of for *h*-MoO_3 was determined to be 187.3 nm. While for the *α*-MoO_3 sheets, the mode of the size frequency distribution was 100 nm (Fig. 3). In addition, Raman spectroscopy spectra confirmed the distinctive structures of the two phases of MoO_3 (Fig. 4). The *h*-MoO_3 Raman spectrum peaks at 135, 173, 216 and 250 cm^{-1} are attributed to the MoO_4 tetrahedra chains. The strong peaks at 316, 397, 491 and 691 cm^{-1} are assigned to the vibrations of O-Mo-O.[28] The Mo=O bond is in the range 889 – 977 cm^{-1}.[28, 30] The *α*-MoO_3 is known for several typical peaks, which are 157, 245, 337, 380, 665, 819 and 994 cm^{-1} in wavenumbers.[29] These vibration peaks are different from the peaks of *h*-MoO_3 and belongs to the high order structure mode, which are very sharp comparing to the peaks in *h*-MoO_3. For instance, the peak at 994 cm^{-1} is assigned to terminal oxygen stretching vibration, which is generated from the unshared oxygen atoms.[26] On the other hand, the peaks 337 and 380 cm^{-1} are O-Mo-O as scissoring vibrations.[29, 31] The FTIR-ATR was also performed to identify the characteristic peak of MoO_3, which was the Mo = O, as previously reported (Fig. S1).[3, 31] Based on these results, the two types of MoO_3 nanoparticles were successfully synthesized.[32] As part of the stability characterization of these nanomaterials, dissolution assays in the fungal growth media were investigated. There

was no significant dissolution observed in czapek media under the conditions used in this study. These results indicate that MoO_3 was stable during the experiments (see supporting information for more information on the dissolution assays and results).

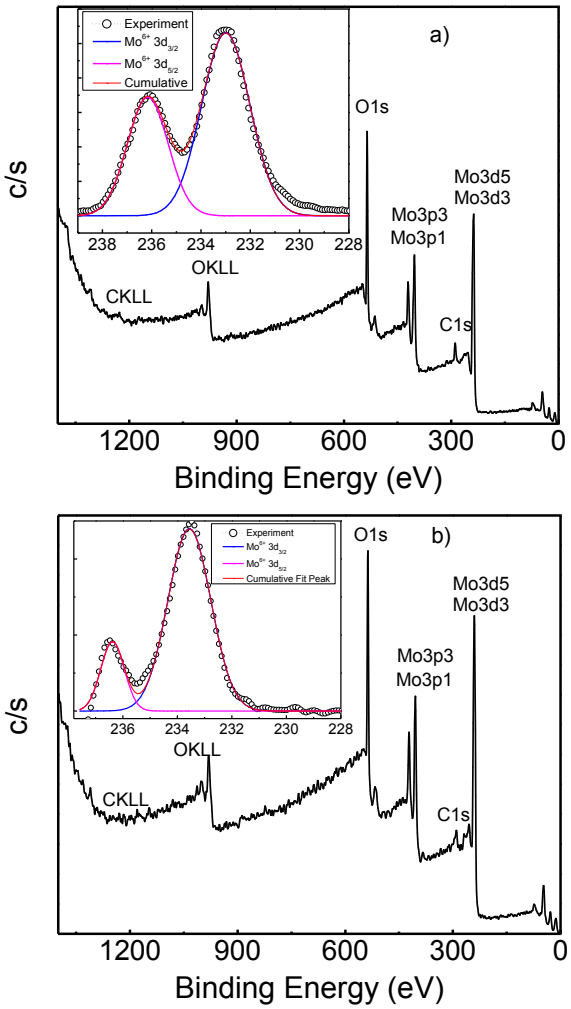

Fig. 2. X-ray Photoelectron Spectroscopy spectra of *h*-MoO_3 (a) and α-MoO_3 (b), the spectra confirmed the successful synthesis of both MoO_3 structures.

Effects of nanoparticles on growth inhibition and morphological changes of A. niger and A. flavus

The initial antifungal comparative analysis of α-MoO_3 and *h*-MoO_3 against *A. niger* and *A. flavus* was determined via biomass growth measurements. The reduction of biomass production was observed for both fungi in the presence of the nanomaterials. The biomass reduction was much more pronounced in the presence of *h*-MoO_3 than α-MoO_3 for both fungi. For instance, the amount of fungal biomass reduction at 10 and 200 mg L^{-1} of α-MoO_3 was 26.9 and 20.9 % for *A. niger* and 1.2 and 12.7 % for *A. flavus*, respectively (Fig. 5). In *A. flavus*, clearly the increasing concentration of the nanomaterial led to decreasing biomass production, this trend was not evident for *A. niger* where higher nanomaterial concentrations did not seem to affect further the biomass production. In the case of *h*-MoO_3, the biomass reduction was 55.0 % and 62.5 % for *A. niger* at 10 and 200 mg L^{-1}, respectively (Fig. 5). In contrast, no reduction was observed at 10 mg L^{-1} *h*-MoO_3 for *A. flavus*, but the reduction was significant (67.4 %) at 200 mg L^{-1} *h*-MoO_3. The results of both MoO_3 nanoparticles showed that *A. niger* was more sensitive to the presence of MoO_3 than *A. flavus* and *h*-MoO_3 was more toxic than α-MoO_3 for both fungi.

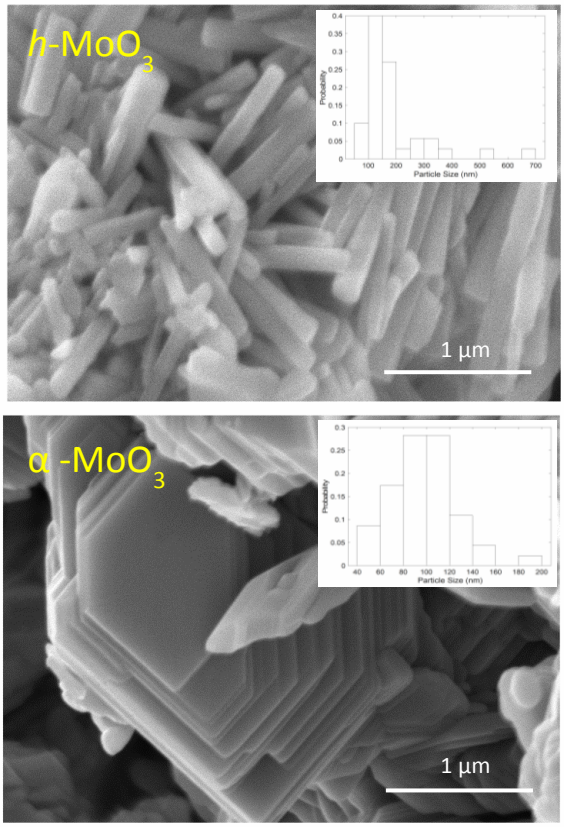

Fig. 3. SEM images showing the characteristic morphologies of *h*-MoO_3 and α-MoO_3 nanoparticles. Scale bar at 1 µm. On top of the SEM images, the histograms show the size distribution of *h*-MoO_3 in diameter and α-MoO_3 in thickness. The mode of the size distribution of the *h*-MoO_3 nanoparticles is around 187.3 nm in diameter; while for α-MoO_3 nanoparticles is 100 nm in thickness.

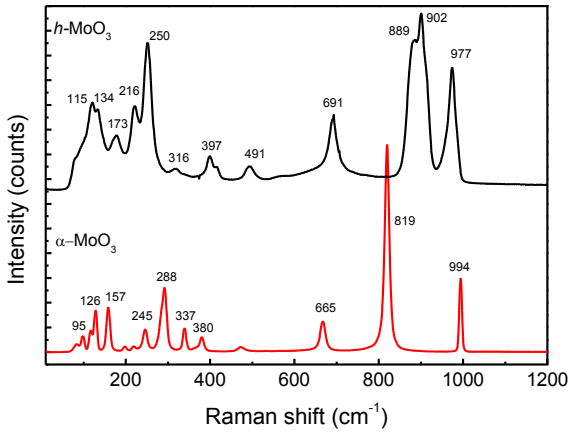

Fig. 4. Raman spectra of of *h*-MoO_3 and α-MoO_3 structure

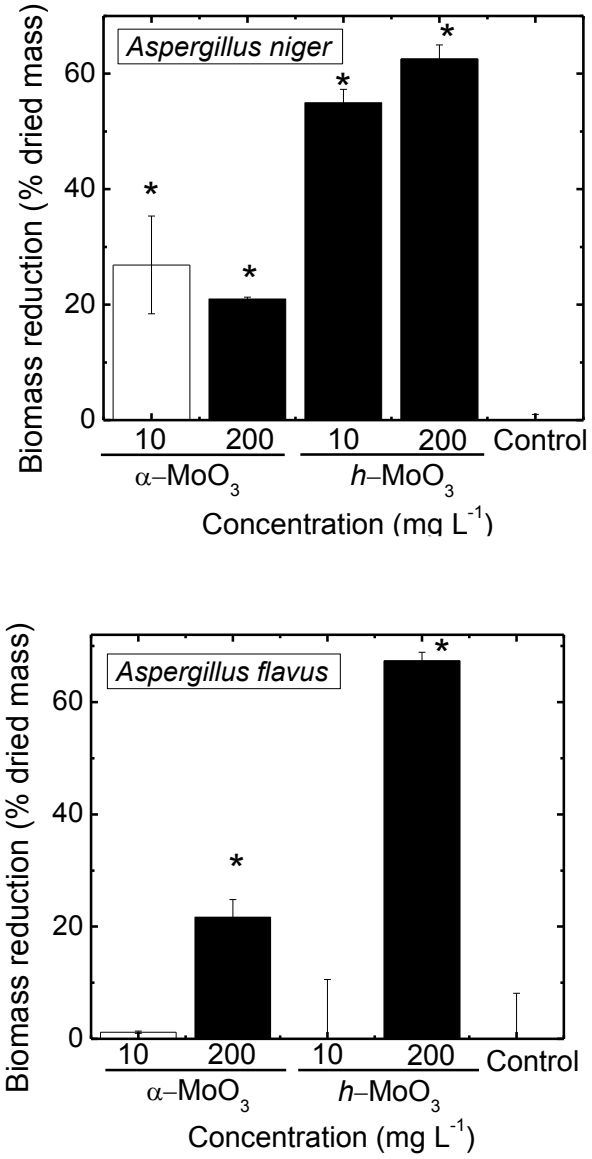

Fig. 5. Biomass reduction (% of dried mass) of *h*-MoO_3 and α-MoO_3 in Czapek media after growing for 10 days. The control samples correspond to the fungal biomass in the growth media without the nanoparticles. The error bars correspond to standard deviations based on three replicates. The symbol (*) means that the sample is statistically different from the control based on T-test analysis.

In terms of mechanisms of antimicrobial property, MoO_3 was previously suggested to interact with the cell-wall of microorganisms.[7, 8, 33] The interaction between MoO_3 and biomolecules, such as amino acids and carbohydrates, of the cell wall is responsible to interrupt the normal development of the hyphae, which could lead to cell disruption.[33] To further investigate the cell-wall interaction with the MoO_3 nanoparticles, we used SEM. The SEM allowed us to compare the hyphae morphological changes in the presence and absence of the nanoparticles. The control samples (no nanoparticles) of both *A. niger* and *A. flavus* presented a smooth hyphae surface, corresponding to normal hyphae. On the other hand, *A. flavus* hyphae treated with *h* and α-MoO_3 presented damaged, shrank and rough surfaces (Fig. 6). These results correlated well with the results of the reduced biomass in the growth inhibition investigation (Fig. 5). In the case of *A. niger*, the treatment with *h*-MoO_3 resulted in more pronounced hyphae changes than with α-MoO_3. The shape of *A. niger* hyphae treated with *h*-MoO_3 was similar to the ones of *A. flavus* treated with both MoO_3 nanoparticles (Fig. 6). This result corroborated well with the biomass growth inhibition observed earlier for both fungal strains (Fig. 5). These results clearly show that the *h*-MoO_3 and α-MoO_3 have different toxicological effects in different fungal strains, however *h*-MoO_3, tends to be more antifungal than α-MoO_3. Previous studies have demonstrated that the antimicrobial activity of nanomaterials is linked to their geometry, dimensions, chemical composition, dissolution stability, surface charge, and polarity. The differences in antifungal activities observed between these two types of nanoparticles are probably because of their different shapes and crystal structures, as previously suggested.[1, 2] For instance, the rod shape of *h*-MoO_3 provides a larger surface area to better interact with the microbial cell wall through physical interactions. Like other nanomaterials, such as graphene nanosheets, [4, 5] it has been reported that MoO_3 can also disrupt the bacterial cell wall as a "blade" cutting through the cell membrane as one of the mechanisms of toxicity toward bacteria.[6] This mechanism could also be considered for fungi, since MoO_3 could play a similar role as a "nano-blade" (α-MoO_3) or "nano-needle" (*h*-MoO_3, rod shape) to puncture the fungal cells generating toxic responses such as the cell deformations observed in the SEM (Fig. 6).

Apoptotic-like cell death responses in the presence of h-MoO_3 and α-MoO_3: mechanism of toxicity

To further understand the physiological response of fungi that led to growth inhibition in the presence of these two nanomaterials, we also investigated apoptotic activity and release of reactive oxygen species (ROS) by the fungi. Fungi produce large amounts of ROS in the presence of antifungal agents or under environmental stress, therefore it is a good marker to determine the stress level caused by MoO_3 nanoparticles to the cells.[36] Another good indicator of stressful conditions to fungi is when the fungus undergoes apoptotic-like cell death, which is defined as a programmed cell death that occurs when conditions are adverse to the fungus. In this study, we investigated early and late apoptosis. Early apoptosis is expressed by nuclear condensation and, in some cases, disappearance of the nuclei in the hyphae. In the case of *A. niger*, the early apoptosis occurred with both MoO_3 nanoparticles with 81% and 74% condensed nuclei of treated hyphae with *h*- and α-MoO_3 respectively. In the control, the nuclei in the hyphae were normal with a round shape and uniformly distributed throughout the hyphae with no condensation (Fig. 7).

The late apoptosis occurs when the early apoptosis of the cells proceeds to the stage that the plasma membrane becomes permeable or loses integrity.[37, 38] In *A. niger,* there was no sign of late apoptosis (Fig. 8). These results suggest that *A. niger* is more resistant to MoO_3 since the apoptosis-like cell death does not progress in *A. niger*. On the other hand, *A.*

flavus presented both late and early apoptosis-like cell death in the presence of MoO_3 nanoparticles. The hyphae presented 85% and 80 % of nuclei condensed with smaller and irregular shape in the presence of *h*- and α-MoO_3 nanoparticles, respectively, comparing to the control (Fig. 6).

In the late apoptosis-like cell death, about 67% of the hyphae allowed the entrance of the blue dye that led to darker blue staining of the hyphae after 5 h exposure to both MoO_3 nanoparticles. These results suggest damage of the cell membrane of the hyphae caused by the presence of the nanomaterials (Fig. 8). Hence, both fungi are affected by the presence of the nanomaterials; however, *A. flavus* was much more sensitive than *A. niger*.

Previous studies have linked the apoptosis-like cell death to fungal production of ROS as a defence mechanism or response to the presence of toxic substances. [39] Therefore, the ROS released from the hyphae to the medium after exposure to the nanomaterial was investigated to determine the toxicity of MoO_3 and its potential role as an indicator for triggering apoptosis-like cell death. The filtrate of the supernatant, after growth for 10 days with the nanomaterials, was analysed for ROS production (Fig. 10 and Fig. 11). The results showed a significant amount of ROS released in the growth medium when the fungi were grown in the presence of MoO_3. The majority of the ROS produced was in the form of H_2O_2 for both *A. niger* and *A. flavus*.

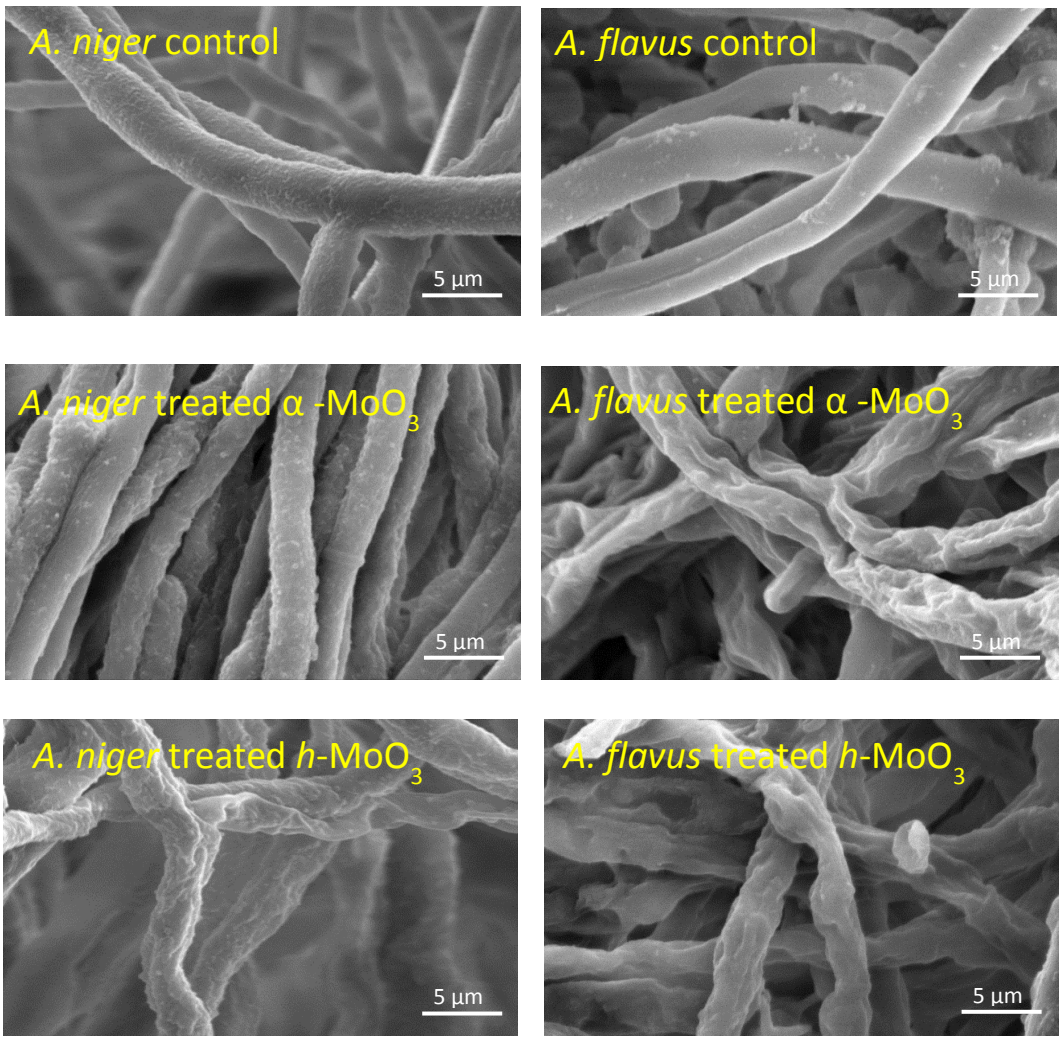

Fig. 6. SEM images of *A. flavus* and *A. niger* exposed to 200 mg L^{-1} of *h*- and α-MoO_3 in Czapek medium after growing for 10 days. The hyphae damage was observed in all samples treated with *h*- and α-MoO_3, except *A. niger* treated with α-MoO_3. The control samples correspond to the fungal biomass in the growth media without the nanoparticles. Scale bar at 5 µm.

The increase of ROS released in the presence of the nanoparticles suggests that the cells were under severe stress, which could have explained the apoptosis-like cell death responses observed earlier in both fungi.

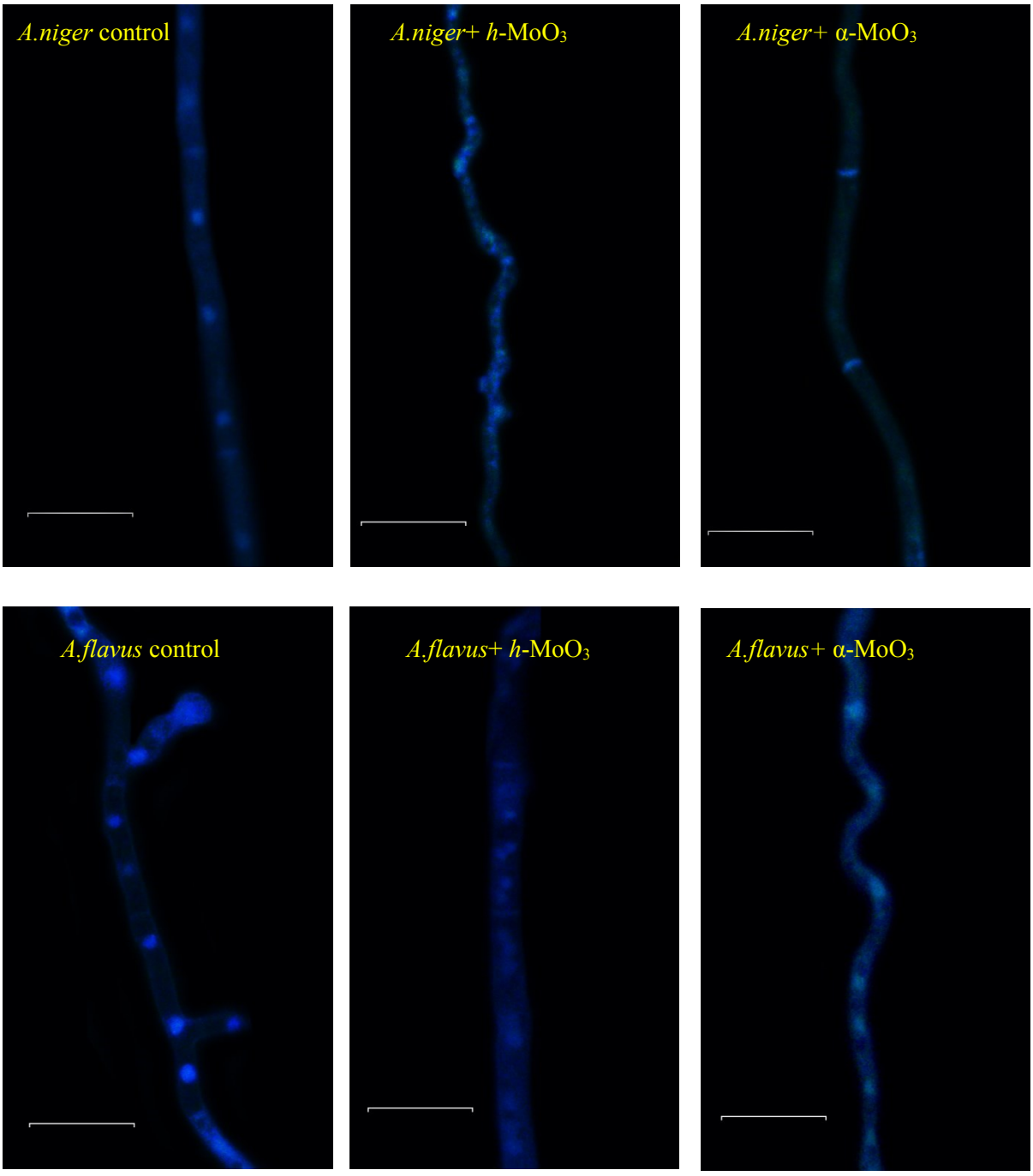

Figure 7. *Aspergillus flavus* and *Aspergillus niger* hyphae treated with *h*- and α-MoO_3 at mg L^{-1}. Conidia were germinated for 5 h at 28°C and then treated for 5 h with *h* and α-MoO_3. The nuclei were stained with Hoechst 33258 (early apoptosis) in bright blue and analysed by fluorescence microscopy. The control samples correspond to the fungal biomass in the growth media without the nanoparticles. Scale bars, 10 µm.

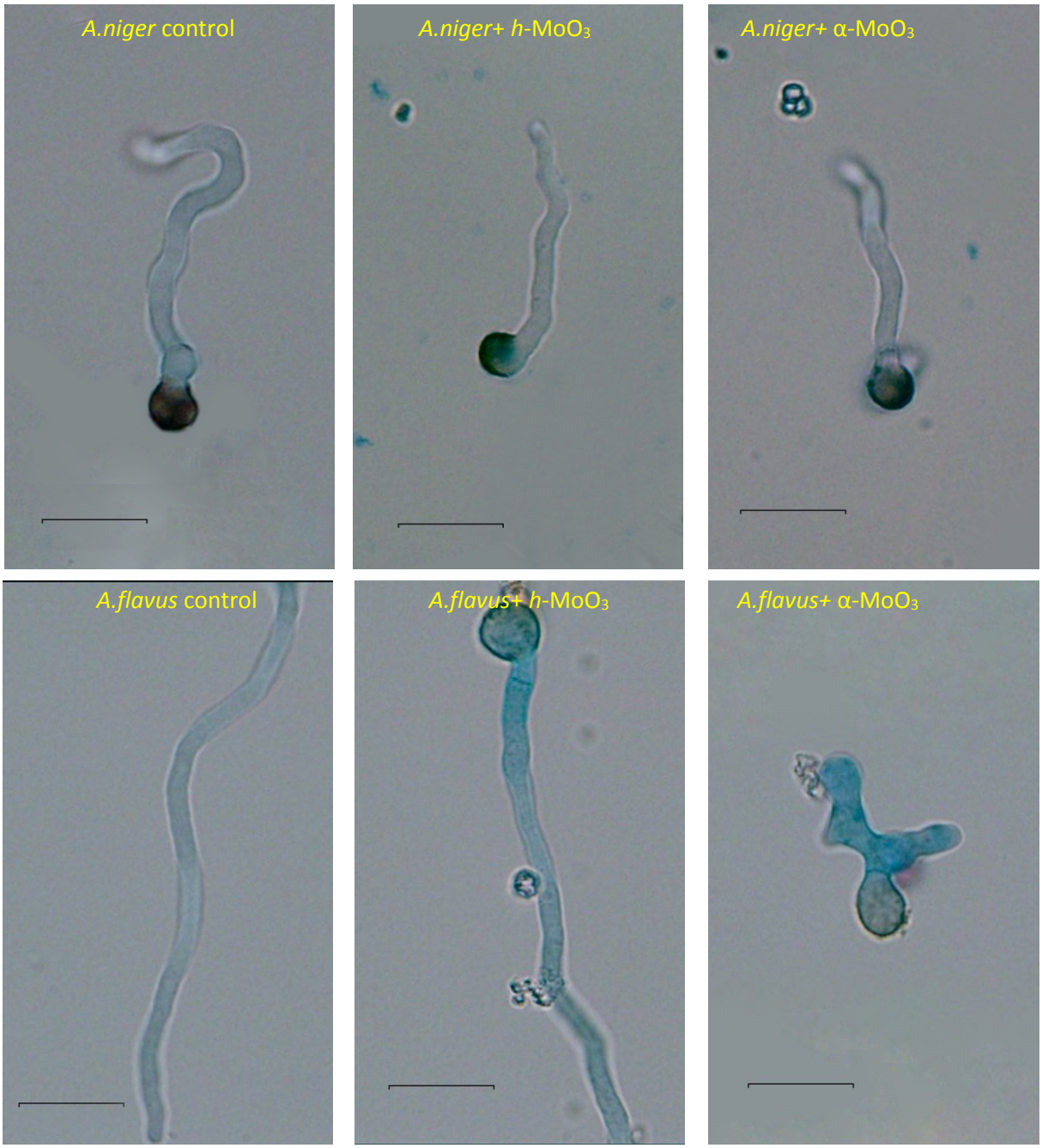

Fig. 8. *Aspergillus flavus* and *Aspergillus niger* hyphae treated with *h* and α-MoO_3 at 200 mg L^{-1}. Conidia were germinated for 5 h at 28°C and then treated for 5 h with *h* and α-MoO_3. The coverslips were stained with Evans Blue (late apoptosis) and analyzed by bright-field microscopy. Blue coloration and growth of the hyphae was observed. The control samples correspond to the fungal biomass in the growth media without the nanoparticles. Scale bars, 10 µm.

Metabolic changes of A. niger and A. flavus in the presence of h-MoO_3 and α-MoO_3

The inhibition of growth, damaged hyphae, ROS production, and apoptosis-like cell death were some of the physiological responses of *Aspergillus* spp. to the presence of MoO_3. These physiological responses are certainly linked to the fungal metabolism. Therefore, to gain a better understanding of the effects of these nanoparticles in the fungal metabolism that are involved in these physiological responses, we also analysed changes in extracellular enzymatic activity and VOC production. The investigation of the enzymatic activity of a microorganism is important to understand its responses to environmental or toxicological changes.[40] *Aspergillus* are well-known to secrete diverse extracellular hydrolytic enzymes, such as protease, lipase, amylase, β-glucosidase, N-acetyl-β-D-glucosaminidase, β-D-glucosidase, naphthol-As-BI-

phosphohydrolase and acid phosphatases and pectinase.[15-19] These enzymes are able to break down extracellular complex compounds into smaller molecules, which could then be up taken by the cell to grow.[46, 47] Therefore, learning more about enzymatic expression changes under the presence or absence of the nanoparticles can determine the metabolic responses of these microorganisms.

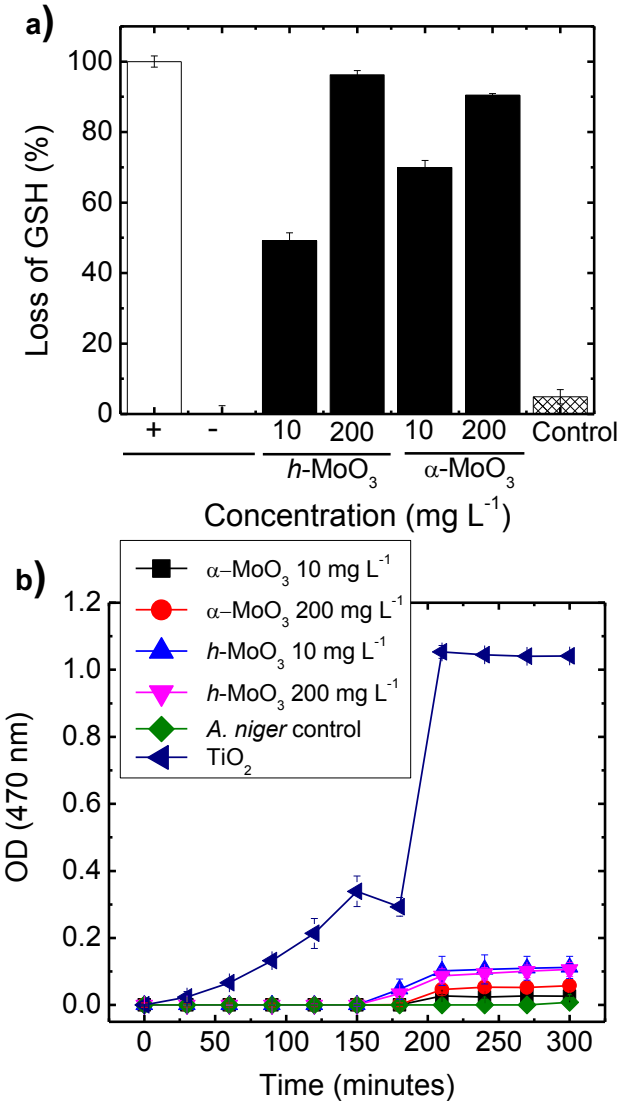

Fig. 9. *Aspergillus niger*: reactive oxygen species (ROS) production over time as (a) H_2O_2 expressed as loss of glutathione and (b) super oxide ($O_2^{\bullet-}$). The control corresponds to the fungi grown without the nanoparticles. The symbols (+) and (-) are controls for the ROS experiment with H_2O_2 only and without H_2O_2. These results show the responses of fungi under stress conditions. The error bars correspond to standard deviations based on three replicates.

In the case of *A. niger*, two enzymes were expressed under normal conditions (no nanoparticles), namely, acid phosphatase and naphthol-As-BI-phosphohydrolase. The production of acid phosphatase was completely inhibited in the presence of both h- and α-MoO_3 (Fig. 11a). This enzyme is an essential enzyme for fungal growth.[48-50] The phosphatase enzyme was previously reported to hydrolyse phosphate monoester to obtain inorganic phosphate and alcohol as end products, in which phosphate is used by the cells.[51] This enzyme is also involved in energy metabolism and signal-transduction pathways and the hydrolysis of glycerophosphate to obtain the necessary phosphorus for fungal growth.[52, 53] Naphthol-As-BI-phosphohydrolase expression was reduced by half in the presence of the nanomaterials (Fig. 11a). This enzyme is in the group of hydrolytic enzymes;[54] therefore, its reduction indicates that the fungi went under stress and reduced its hydrolytic capability. Naphthol-As-BI-phosphohydrolase can also degrade organic phosphorus into inorganic phosphate for the cells.[55, 56] The reduction of enzymatic production was one of the responses of *A. niger* to the presence of MoO_3 and correlates well with the reduced growth of *A. niger* (Fig. 5).

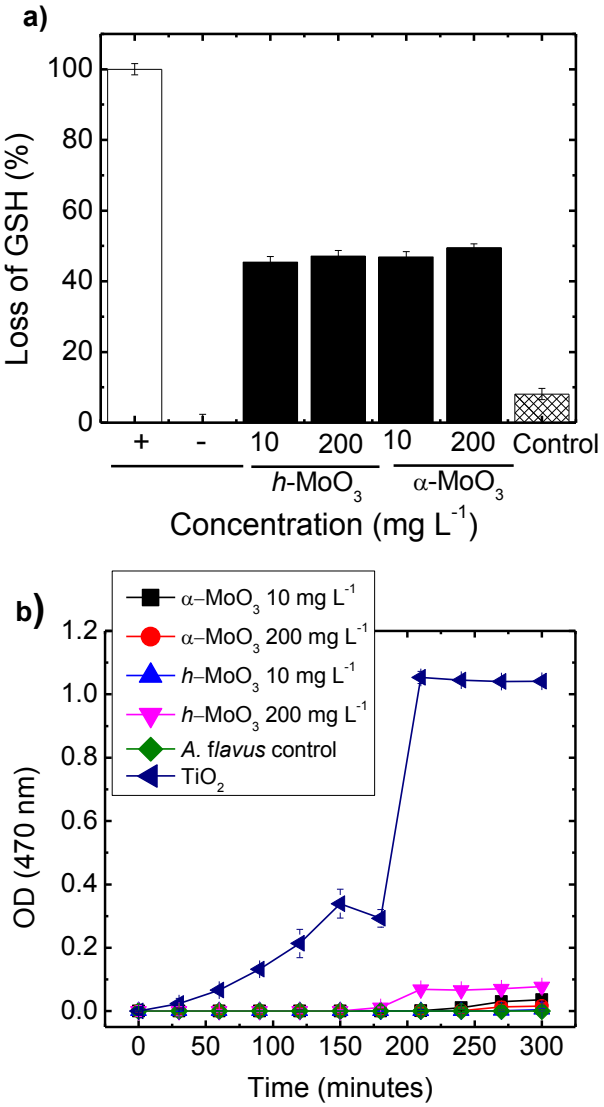

Fig. 10. *Aspergillus flavus*: reactive oxygen species (ROS) production over time as (a) H_2O_2 expressed as loss of glutathione and (b) super oxide ($O_2^{\bullet-}$). The control corresponds to the fungi grown without the nanoparticles. The symbols (+) and (-) are controls for the ROS experiment with H_2O_2 only and without H_2O_2. These results show the responses of fungi under stress conditions. The error bars correspond to standard deviations based on three replicates.

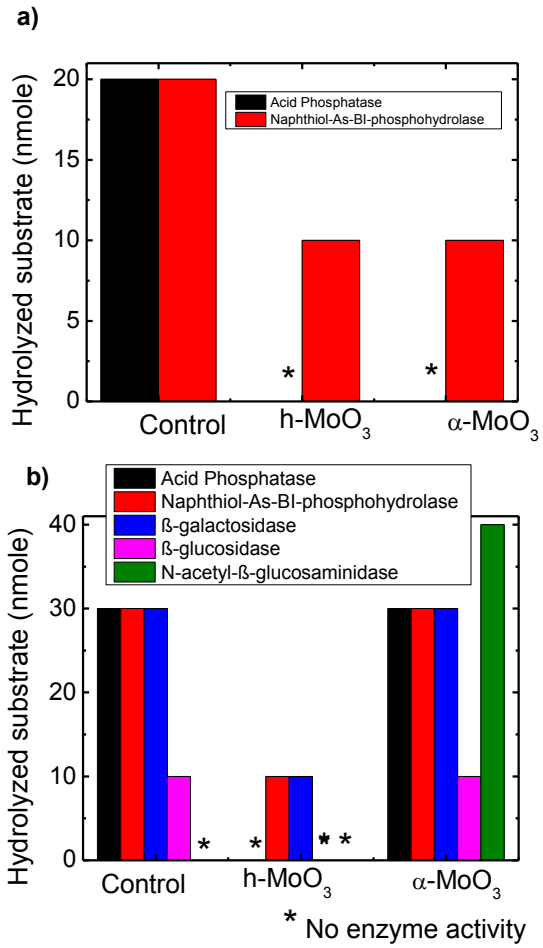

Fig. 11. Enzymatic production by *A. niger* (a) and *A. flavus* (b) in Czapek medium in the presence of *h* and α-MoO_3 at 200 mg L^{-1}. The symbol (*) means that no enzymatic production was observed. Standard deviations are presented, but they were negligible in the figure since the results of the replicates were identical.

In the case of *A. flavus*, a total of four enzymes were produced in the control sample. Like for *A. niger*, *A. flavus* also had significantly reduced activities of both acid phosphatase and naphthol-As-BI-phosphohydrolase enzymes in the presence of h-MoO_3. In addition to these two enzymes, other carbohydrate enzymes (ß-galactosidase and ß-glucosidase) were inhibited or over expressed (N-acetyl-ß-glucosaminidase) in the presence of MoO_3 (Fig. 9). The h-MoO_3 was the nanoparticle that most affected the expression of enzymes. All the enzymes were reduced or not expressed in the presence of h-MoO_3. For instance, the enzyme ß-galactosidase, which is responsible for hydrolysing lactose into glucose and galactose. These carbohydrates are part of the carbohydrate metabolism (glycolysis) of fungi, which ultimately is involved in the energy metabolism.[18, 57] Similarly, ß-glucosidase was not produced by *A. flavus* in the presence of h-MoO_3 (Fig. 11b). This enzyme hydrolyses cellulose into glucose, which can also be used for energy metabolism of these microorganisms. This enzyme together with ß-glucosidase, participate in producing smaller sugars for the energy metabolism of the fungus.[58, 59] It is worth to point out that in the case of *A. flavus* treated with α-MoO_3, there were no changes in the synthesis of the four enzymes as compared to the control (Fig. 11b). In addition to these four enzymes a 5th enzyme was also produced in abundance, N-acetyl-ß-glucosaminidase. This enzyme is not considered essential to fungal growth but is related to morphogenesis. This enzyme is released from the cell to the media when cell death occurs due to autolysis.[60] The presence of this enzyme supports the morphological results of cellular damage and apoptosis-like cell death of *A. flavus* in the presence of α-MoO_3. These results also suggest that the nanomaterials can affect enzymatic production, but their effect seems to be species specific, with the exception of Acid phosphatase and Naphthiol-As-Bi-phosphorhydrolase for h-MoO_3. It is, however, unclear if other species of fungus that also produce these enzymes would have the same responses for these enzymes in the presence of h-MoO_3.

In addition to the enzymatic production, it is well-known that volatile organic compounds (VOCs) produced by fungi consist of a combination of direct products of fungal metabolism and incidental byproducts of substrate degradation.[61] VOCs are typically byproducts of both the primary and secondary metabolisms of fungi. Since VOCs profiles are characteristic of fungal species; they can be used to investigate the species metabolic responses to environmental or toxicological conditions, such as the presence of MoO_3 nanoparticles.[62]

The overall VOC profile of untreated samples showed 25 and 50 different volatile compounds for *A. niger* and *A. flavus*, respectively. These compounds belong mainly to the groups of alcohols, ketones, aldehydes, esters, hydrocarbons, acids and terpenes (Table 1). Within this group, production of alcohol compounds reduced significantly in the presence of MoO_3 for both fungi (Table 1), which indicated lower activities in energy metabolism of the enzymes because alcohol is a byproduct of the phosphate and carbohydrate pathways involving the phosphatase and carbohydrate enzymes (ß-galactosidase and ß-glucosidase) described earlier (Figure 10).[51, 17, 45]

Principal component analyses (PCA) were done to gain a better understanding of the changes in release of VOCs between the controls and the fungi exposed to α-MoO_3 or h-MoO_3 (Fig. 13). The 3-methyl-1-butanol and ethyl alcohol were the compounds that showed the most significant changes in the presence of MoO_3. These alcohols are recognized as *Aspergillus* spp. molecular markers.[63-65] The reduction in the production of these two alcohols by both fungi incidate that the presence of MoO_3 affected the fungal metabolism. In the PCA analysis, clearly different compounds than the controls were expressed in the presence of MoO_3 nanoparticles. Some specific VOCs increased or were produced only in the presence of α-MoO_3 or h-MoO_3 (Fig. 12). For instance, β –Elemene and t-Cadinol in the terpene group, overexpressed in the presence of α-MoO_3 and h-MoO_3 while they did not express or were not significant in the control without nanomaterials. These two VOCs have been previously reported to have antifungal activities.[66, 67] The synthesis of these toxic compounds by both *A. niger* and *A. flavus* in the presence of the two MoO_3

nanoparticles could explain the apoptotic-like cell death responses observed earlier by both fungi.

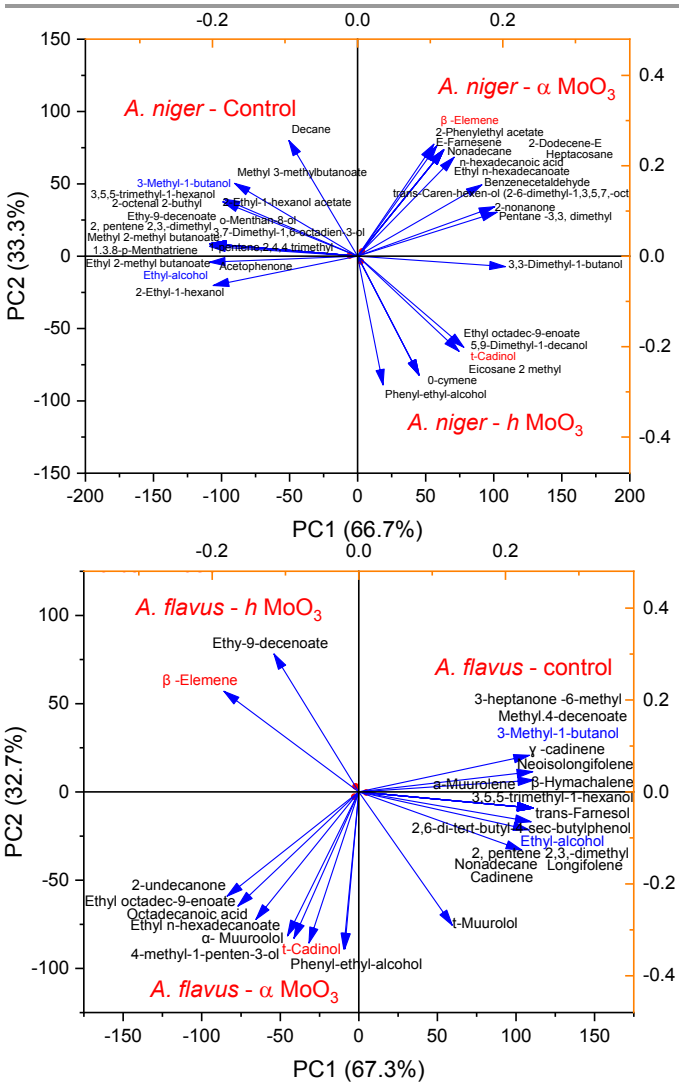

Fig. 12. Principal component analysis (PCA) of the volatile organic compounds (VOCs), released from the *A. niger* (a) and *A. fllavus* (b) exposed to *h*-MoO_3 or α-MoO_3 at 200 mg L^{-1}. The control are the fungi grown without nanomaterials. The VOC names written in blue correspond to the specific biomarkers for the fungi and the VOC names written in red correspond to main antifungal biomarkers produced in the presence of the nanoparticles.

In the case of *A. niger* exposed to h-MoO_3, only six compounds were differently expressed in comparison to the control (Fig. 12). In addition to t-Cadinol, the compound 5,9-Dimethyl-1-decanol is noteworthy to mention because it has been reported to present antifungal activity.[68] In the presence of α-MoO_3, both β –Elemene and Benzenecetaldehyde, which also have antifungal activity,[69] also was overexpressed. In the case of *A. flavus*, the VOCs produced by the control group presented several similarities to the *A. niger* control. Besides 3-methyl-1-butanol and ethyl alcohol, which are produced by both *A. niger* and *A. flavus*, γ -cadinene, another important compound, was abundant only in *A. flavus*.

Table 1: Principal chemical groups of volatile compounds (area relative x 10^6) detected in the head space of the *Aspergillus* spp. cultures grown in liquid Czapek medium at 28°C for 10 days

	Aspergillus niger			***Aspergillus flavus***		
	Control	α-MoO_3	*h*-MoO_3	Control	α-MoO_3	*h*-MoO_3
Alcohols	784.20[a]	254.81[b]	314.89[b]	280.08[a]	141.38[a]	91.25[b]
Ketones	8.69[a]	3.88[ab]	2.07[b]	22.07[a]	20.04[a]	4.61[b]
Aldehydes	18.48[a]	8.61[b]	3.18[b]	n.r	n.r	n.r
Esters	158.47[a]	60.06[b]	36.35[b]	21.49[a]	24.30[a]	14.05[a]
Hydrocarbons	58.13[ab]	97.43[b]	38.03[a]	31.67[a]	4.57[b]	1.09[b]
Acids	n.r	0.12	n.r	0.38[a]	3.06[b]	n.r
Terpenes	6.7[a]	10.87[b]	3.57[a]	646.52[a]	254.28[b]	253.70[b]

[a], [b]: statistically significantly different in comparison to the control; nr: under detection limit

The γ-cadinene (terpene) is also considered to be one of the volatile markers of *A. flavus* (Fig. 13).[70, 71] Alcohols and terpenes are associate with fungal primary and secondary metabolic pathways, respectively. Terpene biosynthesis only happens in the acetate coenzyme A (acetyl-CoA) pathway and are involved in the morphological development of fungi.[72,73, 74] The significant reduction of terpenes (γ-cadinene) in *A. flavus* exposed to MoO_3 suggests lower metabolic activity. These results correlate well with the changes in fungal morphology and lower enzymatic productions discussed earlier. Furthermore, essential VOCs in the *A. flavus* metabolism were inhibited in the presence of h-MoO_3. For instance, Nonadecane and a-Muurolene, which were not detected in the presence of MoO_3, even though they are also considered essential VOCs in Apergillus spp.[75-77] Their inhibition were more pronounced in *A. flavus* than *A. niger*, which corroborates that *A. flavus* is more sensitive to MoO_3 than *A. niger*. Overall, the presence of MoO_3 nanoparticles reduced significantly the production of major biomarkers produced by these organisms under normal growth conditions and impacted their metabolic activities.

These results showed that *h*-MoO_3 was more toxic than α-MoO_3. Their shape and structure only could not have impacted significantly the metabolism of these two microorganisms. Therefore, an additional mechanism is suggested. It is possible that their different chemical composition and reactivity could have played a role as well in the toxicity of these nanoparticles triggering these changes in the fungal metabolism. For instance, *h*-MoO_3 possess a metastable phase while α-MoO_3 has a stable phase.[3] The *h*-MoO_3 has been described to be more active than α-MoO_3 in terms of ability to react with other complex surfaces such as the fungal cell wall. The presence of NH_4^+ ions and water molecules in the structure of *h*-MoO_3 will make it much more readily to interact with other molecules and biomolecules than the α-MoO_3 in aqueous solution.[3] Ammonium ions and water molecules, present in the salt during the synthesis of *h*-MoO_3, are responsible for direction and stabilization of the hexagonal structure of *h*-MoO_3.[1, 3] The transition from *h* to α-MoO_3 removes these two significant structure-directing agents, which results in the stable α-MoO_3

without ammonium ions and water molecules in its structure. The presence of ammonium ions in the *h*-MoO_3 structure has been shown to lead to much higher electrical and ionic conductivity than α-MoO_3.[3] This distinctive electrical-chemical property of *h*-MoO_3 could be responsible for interfering in the normal electrochemical potential of cells, which drives directly the energy metabolism of the cells. In our investigations, we have clearly demonstrated changes in the energy metabolism of these cells when we analysed the changes in expression of enzymes and VOCs by the two fungi. Hence, it is possible that the electrical-chemical properties of these nanomaterials could be responsible for the toxic effects observed in these two microorganisms.

Conclusions

The two types of MoO_3, *h*-MoO_3 and *α*-MoO_3, showed antifungal activities against *Aspergillus niger* and *Aspergillus flavus*. These nanoparticles produced significant changes in the physiology and metabolism of the fungi. The fungal growth and morphological changes observed in the presence of MoO_3 correlated well with the metabolic changes, as determined by the enzymatic and VOC productions. The fungi in the presence of MoO_3 nanoparticles produced ROS and also toxic VOCs that could have triggered the apoptosis-like cell death observed in both fungi. Furthermore, the presence of MoO_3 led to reduction in enzymatic activities of phosphatase and carbohydrate enzymes. These results also indicated that there was an overall reduction in the energy metabolism of *A. niger* and *A. flavus.* The lower enzymatic productions also correlated well with the overall reduction in the production of key volatile compounds from fungal metabolites such as alcohol, aldehyde, hydrocarbons or terpenes. These reductions also confirm the reduction in the metabolic activity of fungi due to the toxicity of MoO_3. In all fungal strains investigated, *h*-MoO_3 showed more pronounced toxicity. Although these fungi belong to the same genus, they did not present similar sensitivity toward MoO_3. *A flavus* seemed more sensitive than *A. niger*. In summary, these results showed that the presence of MoO_3 significantly disrupted the fungal metabolism, which eventually led to slower growth and cell-death. The different toxic levels observed between the two nanoparticles suggest that the toxic responses observed in the two fungi could be because of the structure as well as the electrical-chemical properties and reactivity of the nanoparticles. These findings suggest that MoO_3 can be an alternative antifungal nanomaterial that can alter or slow fungal metabolism by lowering enzymatic activities, shifting the production of volatile organic compounds, and triggering apoptosis-like cell death responses.

Experimental

Fungal preparation

Two fungi were used in this study, namely: *Aspergillus niger* GM31 (University of Teramo, Italy) and *Aspergillus flavus* DSM 62065 (German Culture Collection). Both fungi were cultured on Czapek agar plates (HiMedia Laboratories, LLC, VWR, U.S.A.) from stocks in sterile distilled water. All the cultures were incubated at 28 °C for 5 days in the dark. Then, the fungi were transferred to Czapek agar plates, which were made freshly prior to each experiment and incubated at 28 °C.

Synthesis and characterization of h-MoO_3 and α-MoO_3

The synthesis of *h*-MoO_3 was done following a previously published procedure.[9, 31, 78] The *h*-MoO_3 was synthesized using the precipitation method from acidified ammonium molybdate solution. Briefly, in a 125 mL round bottom flask, ammonium heptamolybdate tetrahydrate (100 mmol, 12.3 g) was stirred with 80 mL deionized water at room temperature until dissolved. Then, 2 M HNO_3 was added dropwise to the solution until pH reached 1. The solution was then heated to 90 °C under constant stirring. After 8 h, the mixture was cooled, and a white precipitate was obtained by vacuum filtration. The white precipitate was washed with water until neutral pH was reached. The white product was then oven dried at 80 °C for 16 h. The white powder, which was the *h*-MoO_3, was cooled and transferred to an amber vial to protect from light. The α-MoO_3 was synthesized using 5 g of *h*-MoO_3, which was transferred to a ceramic evaporating dish. The dish was placed in a furnace and heated at 500 °C for 8 h. The grayish powder, which was the *α*-MoO_3, was cooled and transferred to an amber vial. Both h-MoO_3 and α -MoO_3 were characterized for their crystal structure using X-ray diffraction (XRD) (RIGAKU Miniflex 600), Fourier transform infrared attenuated total reflection (FTIR-ATR, Nicolet iS10), X-ray Photoelectron Spectroscopy (XPS, PHI 5700 X-ray photoelectron spectrometer) Raman spectroscopy (532 nm laser excitation, IHR 320, Horiba) and scanning electron microscopy (SEM, JSM 6010LA, Jeol U.S.A.). The size distribution of the nanoparticles was analysed with ImageJ using 10 SEM images randomly taken in the SEM grid with different magnifications. This technique was used to determine the size distribution of the nanoparticles because these nanoparticles can have different length and diameter dimensions. For instance, *h*-MoO_3 tends to have nano-sized diameters, but larger lengths since they look like needles; and *α*-MoO_3 tends to be nano-sized in thickness, but larger in length, since they look like nanoplatelets. Since MoO_3 nanoparticles have been described to have increasing dissolution at pH 7,[2] dissolution experiments were conducted with the Czapek media and DI water to determine the behaviour of these nanomaterials under the studied conditions (see supporting information).

Mycelial growth inhibition

The sterile *h*-MoO_3 and α-MoO_3 were prepared by placing the nanoparticles under ultraviolet radiation for 20 min (254 nm, Nuaire Labgard biosafety hood cabinet U.S.A). Then, the stock solution was prepared by adding sterile distilled water into the sterile nanomaterials to make up 1000 mg L^{-1} stock solutions. The concentrations of 10 and 200 mg L^{-1} of *h*-MoO_3 and α -MoO_3 were used to investigate the toxicity of *A. flavus* and *A.*

niger. The concentration of 10 mg L^{-1} was selected based on the literature as the highest concentration that gave none or little antimicrobial activity;[23] and 200 mg L^{-1} was selected because this concentration is right above the highest antimicrobial concentration for bacteria and; therefore would take into consideration that fungi is typically more resistant to antimicrobials than bacteria. In 150 mL flask, *h*-MoO_3 and α -MoO_3 stock solutions were added to Czapek medium (pH = 4.63, HiMedia Laboratories) to make up a total volume of 60 mL at the desired concentrations. The controls without nanomaterials or with nanomaterials (but no fungus) were prepared with the same growth medium. Fungi were cultured in Czapek liquid media using a fresh 5-day plate. The mycelium was obtained by centrifuging the grown culture (Thermo Scientific centrifuge) and collecting the fungal pellets for the growth inhibition experiment. The amount of 0.18 g of fungal pellets was introduced to each flask, as described above. The flasks were placed in a shaker at 28 °C and 130 rpm. After ten days, all samples were filtered using a paper filter (Whatman number 5), and then, oven dried at 70 °C for 8 h. The dried biomass was weighed and compared to the controls. All the experiments were prepared in triplicate; then, the results were averaged out and the standard deviation was also recorded. The results were analysed for biomass reduction with the following formula (1).

$$\text{Biomass reduction } (\%) = 100 - \frac{\text{dried mass of the sample}}{\text{dried mass of the control}} \times 100 \quad (1)$$

Fungi enzymatic activity in the presence of h-MoO_3 and α-MoO_3

The production of extracellular enzymes released in the growth medium with and without *h*-MoO_3 or α -MoO_3 was evaluated using API-ZYM® strip (Bio-Merieux, Marcy l'Etoile, France).[41, 43, 79, 80] The growth medium (from the growth reduction experiment described above) was filtered using a 0.22 µm sterile syringe filter (VWR) and then tested for 18 extracellular enzymes (Table S1) enzymes following the API-ZYM Bio-Merieux protocol. Briefly, a volume of 65 µL was placed in each well of the API-ZYM strip. The strips were then incubated in the dark for 4 h at 30 °C. After that, one drop of ZYM A following one drop of ZYM B was added to each well. The enzymatic activity was expressed as nanomoles (nmol) of hydrolyzed substrate based on color intensity of the hydrolyzed materials. The color were interpreted following a color scale of 1 to 5.[81] The sterile Czapek medium was used as negative control.

Apoptotic-like cell death

A. flavus and *A. niger* apoptotic-like cell death in the presence of *h*-MoO_3 and α-MoO_3 were investigated. Controls without nanomaterials were also evaluated at the same time. Both early and late apoptosis were conducted to observe nuclear changes (early apoptosis) and plasm membrane (late apoptosis) of the fungal hyphae, respectively.[82] For early apoptosis, the hyphae were stained with 0.5 mg mL^{-1} Hoechst 33258 freshly prepared (Sigma-Aldrich, U.S.A.). Additionally, a fresh fixation solution was prepared in 1x phosphate buffer solution (PBS, 0.2M, pH = 7.4, Sigma Aldrich, U.S.A.) with dimethyl sulfoxide (DMSO, 5 %) and formaldehyde (3.7 %). Another solution was prepared in 1x PBS with glycerol (5 %) and *n*-propyl-gallate (0.1 %) for the slide mounting process and stored as aliquots at -20 °C.

For the slide preparation, 100 µL of spores grown in Czapek medium from a 5-day fungal plate (3.5 x 10^5 spore mL^{-1}) was placed on sterile coverslips (22 mm x 22 mm) in triplicate. All the samples were incubated at 28 °C for 5 h. And then, 100 µL of 200 mg L^{-1} *h*-MoO_3 or α -MoO_3 were added to the coverslips. The negative control was prepared by adding 100 µL of sterile DI water to the spores instead of nanoparticles. All the samples were incubated at 28 °C for 5 h followed by the staining process. The fixation solution (500 µL) was allowed to react for 15 min at 24 °C in the coverslip. Following fixation, the samples were washed three times for 5 min with 10 mL of 1x PBS. After that, the nuclei were stained for 5 min with 500 µL staining solution. The coverslips were washed with sterile distilled water following by blotting drying the edges with Kimwipe. The last step was to mount the sample over a microscopic glass slide with 10 µL of the mounting solution. Finally, the coverslip was secured with nail polish. The fluorescence images were obtained to observe the hypha nuclei using BX 51 Olympus Fluorescence Microscope (Leeds Instrument Inc.) equipped with a DP72 digital camera and DAPI (4',6-diamidino-2-phenylindole) filter. A total of 12 images for each sample were taken to observe changes in the nuclei. The total number of normal nuclei and condensed nuclei of each sample was calculated to estimate the percentage of nucleus condensation.

For late apoptosis, the plasma integrity was determined using Evans Blue (Sigma-Aldrich). Immediately before the experiment, Evans Blue was prepared at 1 % in 1x PBS. The cover slips with the fungi were prepared as described in the early apoptosis section. And then, 1 mL of Even Blue was added to the samples and allowed to stain for 5 min. After that, the same procedure for washing and mounting as described earlier were employed for late apoptosis. There was a total of 12 bright field images (BX 51 Olympus) obtained to determine colour changes of the fungal hyphae. The number of stained images and unstained images was determined to calculate the percentage of hyphae in late apoptosis.

Fungus morphological changes in the presence of h-MoO_3 and α-MoO_3

The morphological changes of the hyphae were investigated using Scanning Electron Microscopy (SEM). Both fungi were grown following the same procedures described earlier. And then, the fungi were collected for fixation with 2.5 % glutaraldehyde solution at 4 °C for 24 h in the dark.[83, 84] After 24 h, the samples were washed twice for 15 min with 1x PBS. The post-fixation consisted in incubating the sample for 2 h at 24 °C with 1 % osmium tetraoxide (Sigma Aldrich, U.S.A.). Osmium tetraoxide presents acute toxicity via oral, inhalation or dermal contact; thus, it should be handled with extreme caution. Following two washes with PBS to complete the post–

fixation, the dehydration step with ethanol/water (v/v %) was conducted with 50 % for 10 min, 70 % for 10 min, 95 % for 5 min and 100 % for 1 min. After that, a serial step of rinses with different ratios of acetone/ethanol, was carried out twice at 1:2, 1:1 and 2:0 for 30 s for each ratio. After rinsing, the fungi were dried at room temperature and sputter coated with gold (Denton V, U.S.A.) for 40 s at 45 mAmps before capturing SEM images (JSM 6010LA, Jeol U.S.A.).

Thiol oxidation assay for reactive oxygen species (ROS) production by the fungi

An indirect method, called Ellman's assay, was used to determine the production of reactive oxygen species in this study.[85-88] ROS assay was employed to investigate the generation of ROS by the fungi in the presence of *h*-MoO_3 and α-MoO_3. In the growth inhibition experiment, the hyphae filtrate was further filtered using a 0.22 µm syringe filter. And then, the Ellman's assay was carried by adding 225 µL of medium filtrate and 225 µL of GSH in 2 mL tube. The glutathione (GSH) was prepared at 0.4 mM in 50 mM bicarbonate buffer ($NaHCO_3$, pH = 8.6). A volume of 225 µL of each sample, *i.e.* fungal filtrate with 10 and 200 mg L^{-1} of *h*-MoO_3 or α -MoO_3, negative control as bicarbonate buffer and 30 % hydrogen peroxide as positive control were added to 225 µL GSH and then incubated at room temperature for 2 h at 150 rpm. The percentage loss of GSH was recorded as the production of ROS by the fungi. All the experiments were prepared in triplicate. The following formula was employed to calculate the loss of GSH as described in a previous study.[89]

$$\text{Loss of GSH (\%)} = \frac{(\text{absorbance of negative control} - \text{absorbance of sample})}{\text{absorbance of negative control}} \text{ x } 100$$

Superoxide radical anion ($O_2^{-\cdot}$)

The filtrate from growing fungi with and without h-MoO3 and α-MoO3 were tested for the production of $O_2^{-\cdot}$. The tetrazolium dye XTT assay (2,3-Bis(2-methoxy-4-nitro-5-sulfophenyl)-2H-tetrazolium-5-carboxanilide inner salt, Biotium, U.S.A.) was used for the measurement of the superoxide radical anion. Phenazine methylsulfate (PMS) was used as activated agent following the protocol from Biotium. XTT is one of the most common methods used in cell culture to detect the presence of $O_2^{-\cdot}$.[90-92] The ratio of 1 : 3 of XTT : samples, which included medium filtrate and negative controls (XTT and samples without XTT) were prepared. All the samples were placed in black 96-well plates in the dark. TiO_2 was used as a positive control, which was activated continuously with UV light (UV light activated, BLE-480B, Spectroline, U.S.A). All the samples were read every 30 min at 470 nm for a total of 300 min (Synergy MX Microtiter, Biotek, U.S.A). The final results were the absorbance after subtracting from the background of negative controls.

Production of volatile organic compounds (VOCs)

The fungal growth samples were prepared with the same procedure described earlier in the growth inhibition section. After that, the medium supernatant was processed as previously described.[63] The VOCs in the headspace were analysed using solid phase micro-extraction (SPME) connected to gas chromatography mass spectrometry (GC-MS).[93] There was an exposing period of 50 min at 45°C of the SPME fibre (75 mm, carboxen/polydimethylsiloxane, CAR/PDMS) to the headspace before injection to the GC inlet. This holding time was based on prior optimization of the extraction conditions.

For detection and separation of the peaks, an Agilent Hewlett-Packard 6890 GC equipped with a MS detector 5970 MSD (Hewlett-Packard, Geneva, Switzerland) was used. A fused silica capillary column (CP-Wax 52 CB, 50 m x 0.32 mm, Chrompack, Middelburg, The Netherlands), coated with polyethylene glycol (film thickness 1.2 µm) was used as stationary phase. The injector and Flame Ionization Detector temperature were at 250 °C and the detector temperature was at 220 °C. Carrier gas (helium) was kept at 1 mL min^{-1} flow rate. The temperature program was set as following: oven temperature started once the fibre was introduced, holding temperature as 40 °C for 2 min, using ramp 10 °C per min to 200 °C, following a ramp of 15 °C per min from 200 to 250 °C and the final holding temperature at 250 °C for 5 min.

The peaks of the profile were identified using computer matching of mass spectral data to the compounds in the library of the mass spectral database (Agilent Hewlett-Packard NIST 98 and Wiley version 6, probability set at >90%). Standards (Sigma Aldrich, Taufkirchen, Germany) were used to identify the positive volatile compounds detected in the samples. The quantities of the compounds were showed as relative areas, which were compared to the areas of the controls (no inoculation). Then, the principal component analysis (PCA) was performed for all the VOC data obtained with the fungi using the OriginLab software.

Conflicts of interest

There are no conflicts to declare.

Acknowledgements

The authors want to thank the undergraduate students M. Padua for assisting with the apoptosis images. This project was funded by the U.S. Department of Energy: Biological and Environmental Research Science Focus Area grant (grant no. DE-AC52-06NA25396) and NSF BEINM Grant Number: 1705511.

References

1. P. Wongkrua, T. Thongtem and S. Thongtem, *Journal of Nanomaterials*, 2013, 2013, 8.
2. L. Cheng, M. Shao, X. Wang and H. Hu, *Chemistry – A European Journal*, 2009, 15, 2310-2316.

3. A. Chithambararaj, N. Rajeswari Yogamalar and A. C. Bose, *Crystal Growth & Design*, 2016, 16, 1984-1995.
4. W. Tang, L. Liu, S. Tian, L. Li, Y. Yue, Y. Wu and K. Zhu, *Chemical Communications*, 2011, 47, 10058-10060.
5. K. Hermann, M. Witko and A. Michalak, *Catalysis Today*, 1999, 50, 567-577.
6. C. Zollfrank, K. Gutbrod, P. Wechsler and J. P. Guggenbichler, *Materials Science and Engineering: C*, 2012, 32, 47-54.
7. K. Krishnamoorthy, M. Premanathan, M. Veerapandian and S. J. Kim, *Nanotechnology*, 2014, 25, 315101.
8. K. Krishnamoorthy, M. Veerapandian, K. Yun and S. J. Kim, *Colloids and surfaces. B, Biointerfaces*, 2013, 112, 521-524.
9. H. N. Nguyen, E. T. Nadres, B. G. Alamani and D. F. Rodrigues, *Journal of Materials Chemistry B*, 2017, 5, 6616-6628.
10. A. Fakhri and P. A. Nejad, *Journal of Photochemistry and Photobiology B: Biology*, 2016, 159, 211-217.
11. S. H. Chotirmall, M. Al-Alawi, B. Mirkovic, G. Lavelle, P. M. Logan, C. M. Greene and N. G. McElvaney, *BioMed research international*, 2013, 2013.
12. M. T. Hedayati, A. C. Pasqualotto, P. A. Warn, P. Bowyer and D. W. Denning, *Microbiology*, 2007, 153, 1677-1692.
13. A. Yoshimi, K. Miyazawa and K. Abe, *Bioscience, biotechnology, and biochemistry*, 2016, 80, 1700-1711.
14. R. P. de Vries, R. Riley, A. Wiebenga, G. Aguilar-Osorio, S. Amillis, C. A. Uchima, G. Anderluh, M. Asadollahi, M. Askin and K. Barry, *Genome biology*, 2017, 18, 28.
15. A. K. Person, S. M. Chudgar, B. L. Norton, B. C. Tong and J. E. Stout, *Journal of Medical Microbiology*, 2010, 59, 834-838.
16. B. Kendrick, in *eLS*, John Wiley & Sons, Ltd, 2001, DOI: 10.1002/9780470015902.a0002320.pub2.
17. E. Moore-Landecker, in *eLS*, John Wiley & Sons, Ltd, 2001, DOI: 10.1002/9780470015902.a0000378.pub2.
18. E. Schuster, N. Dunn-Coleman, J. Frisvad and P. van Dijck, *Applied Microbiology and Biotechnology*, 2002, 59, 426-435.
19. K. Gulshan and W. S. Moye-Rowley, *Eukaryotic Cell*, 2007, 6, 1933-1942.
20. A. Chithambararaj and A. C. Bose, *Beilstein journal of nanotechnology*, 2011, 2, 585-592.
21. A. Chithambararaj and A. C. Bose, *Journal of Alloys and Compounds*, 2011, 509, 8105-8110.
22. Y. Jin-Peng, W. Wen-Qing, C. Li-Wen, L. Yan-Qing, T. Jian-Xin, K. Satoshi, U. Nobuo and Z. Xiang-hua, *Journal of Physics: Condensed Matter*, 2016, 28, 185502.
23. S. Dhanavel, E. A. K. Nivethaa, K. Dhanapal, V. K. Gupta, V. Narayanan and A. Stephen, *RSC Advances*, 2016, 6, 28871-28886.
24. X. W. Lou and H. C. Zeng, *Chemistry of Materials*, 2002, 14, 4781-4789.
25. B. Baker, T. P. Feist and E. M. McCarron Iii, *Journal of Solid State Chemistry*, 1995, 119, 199-202.
26. B. Hui, G. Li, X. Zhao, L. Wang, D. Wu, J. Li and B. K. Via, *Journal of Materials Science: Materials in Electronics*, 2017, 28, 3264-3271.
27. C. C. Zhang, L. Zheng, Z. M. Zhang, R. C. Dai, Z. P. Wang, J. W. Zhang and Z. J. Ding, *physica status solidi (b)*, 2011, 248, 1119-1122.
28. A. Phuruangrat, J. Chen, X. Lou, O. Yayapao, S. Thongtem and T. Thongtem, *Applied Physics A: Materials Science & Processing*, 2012, 107, 249-254.
29. S. Dhanavel, E. A. K. Nivethaa, K. Dhanapal, V. K. Gupta, V. Narayanan and A. Stephen, *RSC Advances*, 2016, 6, 28871-28886.
30. S. Bai, S. Chen, L. Chen, K. Zhang, R. Luo, D. Li and C. C. Liu, *Sensors and Actuators B: Chemical*, 2012, 174, 51-58.
31. A. Chithambararaj, N. S. Sanjini, A. C. Bose and S. Velmathi, *Catalysis Science & Technology*, 2013, 3, 1405-1414.
32. Z. Wang, W. Zhu, Y. Qiu, X. Yi, A. von dem Bussche, A. Kane, H. Gao, K. Koski and R. Hurt, *Chemical Society Reviews*, 2016, 45, 1750-1780.
33. N. Desai, S. Mali, V. Kondalkar, R. Mane, C. Hong and P. Bhosale, *Journal of Nanomedicine & Nanotechnology*, 2015, 6, 1.
34. L. Ou, B. Song, H. Liang, J. Liu, X. Feng, B. Deng, T. Sun and L. Shao, *Particle and Fibre Toxicology*, 2016, 13, 57.
35. M. Fojtů, W. Z. Teo and M. Pumera, *Environmental Science: Nano*, 2017, 4, 1617-1633.
36. D. Carmona-Gutierrez, T. Eisenberg, S. Buttner, C. Meisinger, G. Kroemer and F. Madeo, *Cell Death Differ*, 2010, 17, 763-773.
37. I. K. H. Poon, M. D. Hulett and C. R. Parish, *Cell Death And Differentiation*, 2009, 17, 381.
38. V. A. Patel, A. Longacre, K. Hsiao, H. Fan, F. Meng, J. E. Mitchell, J. Rauch, D. S. Ucker and J. S. Levine, *The Journal of biological chemistry*, 2006, 281, 4663-4670.
39. A. Hamann, D. Brust and H. D. Osiewacz, *Trends in Microbiology*, 2008, 16, 276-283.
40. J. Weglowska, A. Reich, B. Walów and J. C. Szepietowski, *International Journal of Biomedical Science : IJBS*, 2006, 2, 29-33.
41. P. C. Jain, J. Lacey and L. Stevens, *Mycological Research*, 1991, 95, 834-842.
42. H. L. Hu, J. van den Brink, B. S. Gruben, H. A. B. Wösten, J. D. Gu and R. P. de Vries, *International Biodeterioration & Biodegradation*, 2011, 65, 248-252.
43. S. Alam, H. Shah and N. Magan, *World Mycotoxin Journal*, 2009, 2, 313-322.
44. N. Magan and D. Aldred, 2008.
45. J. E. Mellon, P. J. Cotty and M. K. Dowd, *Applied Microbiology and Biotechnology*, 2007, 77, 497-504.
46. E. A. Whitehead and S. N. Smith, *Enzyme and Microbial Technology*, 1989, 11, 736-743.
47. R. S. Sinsabaugh, *Biology and Fertility of Soils*, 1994, 17, 69-74.
48. J. C. Tarafdar, R. S. Yadav and S. C. Meena, *Journal of Plant Nutrition and Soil Science*, 2001, 164, 279-282.
49. C. J. Straker and D. T. Mitchell, *The New Phytologist*, 1986, 104, 243-256.
50. W. Wang, Y. Li, H. Wang and Y. Zu, *PLOS ONE*, 2014, 9, e111740.
51. J. B. Vincent, M. W. Crowder and B. A. Averill, *Trends in Biochemical Sciences*, 1992, 17, 105-110.
52. L. H. Guimaraes, H. F. Terenzi, J. A. Jorge, F. A. Leone and L. Polizeli Mde, *Biotechnology and applied biochemistry*, 2004, 40, 201-207.
53. G. Tasnadi, M. Zechner, M. Hall, K. Baldenius, K. Ditrich and K. Faber, 2017, 114, 2187-2195.

54. J. J. Amberg, N. R. Jensen, R. A. Erickson, B. Sauey and C. Jackson, *Ichthyological Research*, 2018, 65, 245-251.
55. B. W. Sauey, J. J. Amberg, S. T. Cooper, S. K. Grunwald, R. J. Haro and M. P. Gaikowski, *Journal of Freshwater Ecology*, 2016, 31, 303-314.
56. R. C. Oliveira, R. R. Oliveira, C. M. Bordon, D. J. Tessmann, K. R. F. Schwan-Estrada and J. B. Vida, *Journal of Phytopathology*, 2013, 161, 210-212.
57. A. Sørensen, M. Lübeck, P. S. Lübeck and B. K. Ahring, *Biomolecules*, 2013, 3, 612-631.
58. X. Hu, S. Robin, S. O'Connell, G. Walsh and J. G. Wall, *Applied Microbiology and Biotechnology*, 2010, 87, 1773-1782.
59. Z. Wen, W. Liao and S. Chen, *Applied biochemistry and biotechnology*, 2005, 121-124, 93-104.
60. T. Pusztahelyi and I. Pócsi, *Acta Microbiologica et Immunologica Hungarica*, 2014, 61, 131-143.
61. K. K. Pennerman, H. S. Al-Maliki, S. Lee and J. W. Bennett, in *New and Future Developments in Microbial Biotechnology and Bioengineering*, Elsevier, Amsterdam, 2016, DOI: https://doi.org/10.1016/B978-0-444-63505-1.00007-5, pp. 95-115.
62. D. Freihorst, M. Brunsch, S. Wirth, K. Krause, O. Kniemeyer, J. Linde, M. Kunert, W. Boland and E. Kothe, *Fungal Genetics and Biology*, DOI: https://doi.org/10.1016/j.fgb.2016.08.007.
63. C. P. Costa, D. Gonçalves Silva, A. Rudnitskaya, A. Almeida and S. M. Rocha, *Scientific Reports*, 2016, 6, 27441.
64. M. Ndagijimana, C. Chaves-Lopez, A. Corsetti, R. Tofalo, M. Sergi, A. Paparella, M. E. Guerzoni and G. Suzzi, *International journal of food microbiology*, 2008, 127, 276-283.
65. M. Kuske, A.-C. Romain and J. Nicolas, *Building and Environment*, 2005, 40, 824-831.
66. S. A. Siddiqui, R. Islam, R. Islam, A. H. M. Jamal, T. Parvin and A. Rahman, *Arabian Journal of Chemistry*, 2017, 10, S2170-S2174.
67. E. Sieniawska, R. Sawicki, J. Golus and M. Swatko-Ossor, 2018, 23.
68. W. Arango, J. Miguel Acevedo Ruíz and C. Pelaez, *Fungicidal activity of Eucalyptus tereticornis essential oil on the pathogenic fungus Fusarium oxysporum*, 2011.
69. M. Kobaisy, M. R. Tellez, C. L. Webber, F. E. Dayan, K. K. Schrader and D. E. Wedge, *Journal of agricultural and food chemistry*, 2001, 49, 3768-3771.
70. H. J. Zeringue, D. Bhatnagar and T. E. Cleveland, *Applied and Environmental Microbiology*, 1993, 59, 2264-2270.
71. V. Polizzi, A. Adams, S. V. Malysheva, S. De Saeger, C. Van Peteghem, A. Moretti, A. M. Picco and N. De Kimpe, *Fungal Biology*, 2012, 116, 941-953.
72. A. G. Simon, D. K. Mills and K. G. Furton, *Journal of Chromatography A*, 2017, 1487, 72-76.
73. N. P. Keller, G. Turner and J. W. Bennett, *Nature Reviews Microbiology*, 2005, 3, 937.
74. J. C. R. Demyttenaere, A. Adams, K. Van Belleghem, N. De Kimpe, W. A. König and A. V. Tkachev, *Phytochemistry*, 2002, 59, 597-602.
75. A. Müller, P. Faubert, M. Hagen, W. zu Castell, A. Polle, J.-P. Schnitzler and M. Rosenkranz, *Fungal Genetics and Biology*, 2013, 54, 25-33.
76. S. Siddiquee, S. A. Azad, F. Abu Bakar, L. Naher and S. Vijay Kumar, *Journal of Saudi Chemical Society*, 2015, 19, 243-256.
77. H. Jeleń and E. Wasowicz, *Food Reviews International*, 1998, 14, 391-426.
78. A. Chithambararaj, N. S. Sanjini, S. Velmathi and A. Chandra Bose, *Physical Chemistry Chemical Physics*, 2013, 15, 14761-14769.
79. P. Zorzete, R. C. Oliveira and B. Corrêa, *Journal of Food Safety*, 2016, 36, 467-473.
80. R. C. Oliveira, H. N. Nguyen, C. A. Mallmann, R. S. Freitas, B. Correa and D. F. Rodrigues, *Science of The Total Environment*, 2018, 640-641, 1132-1138.
81. M. Jimenez, R. Mateo, A. Querol, J. J. Mateo and E. Hernandez, *Appl Environ Microbiol*, 1990, 56, 3718-3722.
82. C. P. Semighini and S. D. Harris, in *Molecular and Cell Biology Methods for Fungi*, ed. A. Sharon, Humana Press, Totowa, NJ, 2010, DOI: 10.1007/978-1-60761-611-5_20, pp. 269-279.
83. S. Thabet, F. Simonet, M. Lemaire, C. Guillard and P. Cotton, *Applied and Environmental Microbiology*, 2014, 80, 7527-7535.
84. G. Helal, M. Sarhan, A. Abu Shahla and E. Abou El-Khair, *Journal of Basic Microbiology*, 2007, 47, 5-15.
85. G. L. Ellman, *Archives of biochemistry and biophysics*, 1959, 82, 70-77.
86. S. B. Liu, T. H. Zeng, M. Hofmann, E. Burcombe, J. Wei, R. R. Jiang, J. Kong and Y. Chen, *Acs Nano*, 2011, 5, 6971-6980.
87. H. N. Nguyen, E. T. Nadres, B. G. Alamani and D. F. Rodrigues, *Journal of Materials Chemistry B*, 2017, 5, 6616-6628.
88. J. Peña-Bahamonde, V. San Miguel, H. N. Nguyen, R. Ozisik, D. F. Rodrigues and J. C. Cabanelas, *Carbon*, 2017, 111, 258-268.
89. S. Liu, T. H. Zeng, M. Hofmann, E. Burcombe, J. Wei, R. Jiang, J. Kong and Y. Chen, *Acs Nano*, 2011, 5, 6971-6980.
90. M. W. Sutherland and B. A. Learmonth, *Free radical research*, 1997, 27, 283-289.
91. M. V. Berridge and A. S. Tan, *Protoplasma*, 1998, 205, 74-82.
92. J. Fan, Y. Li, H. N. Nguyen, Y. Yao and D. F. Rodrigues, *Environmental Science: Nano*, 2015, 2, 370-379.
93. C. Chaves-Lopez, A. Serio, A. Gianotti, G. Sacchetti, M. Ndagijimana, C. Ciccarone, A. Stellarini, A. Corsetti and A. Paparella, *Journal of applied microbiology*, 2015, 119, 487-499.

1